GA–A27919

FULL-F NEOCLASSICAL SIMULATIONS TOWARD A PREDICTIVE MODEL FOR H-MODE PEDESTAL ION ENERGY, PARTICLE AND MOMENTUM TRANSPORT

by

D.J. BATTAGLIA, J.A. BOEDO, K.H. BURRELL, C.S. CHANG, J.M CANIK,
J.S. DEGRASSIE, S.P. GERHARDT, B.A. GRIERSON, R.J. GROEBNER,
R. MAINGI, AND S.P. SMITH

OCTOBER 2014

GENERAL ATOMICS

DISCLAIMER

GA–A27919

FULL-F NEOCLASSICAL SIMULATIONS TOWARD A PREDICTIVE MODEL FOR H-MODE PEDESTAL ION ENERGY, PARTICLE AND MOMENTUM TRANSPORT

by

D.J. BATTAGLIA[1], J.A. BOEDO[2], K.H. BURRELL[3], C.S. CHANG[1], J.M CANIK[4], J.S. DEGRASSIE[3], S.P. GERHARDT[1], B.A. GRIERSON[1], R.J. GROEBNER[3], R. MAINGI[1], AND S.P. SMITH[3]

This is a preprint of the synopsis for a paper to be presented at the Twenty-Fifth IAEA Fusion Energy Conf., October 13-18, 2014 in Saint Petersburg, Russia.

[1]Princeton Plasma Physics Laboratory, Princeton, New Jersey, USA
[2]University of California, San Diego, La Jolla, California, USA
[3]General Atomics, P.O. Box 85608, San Diego, California, USA
[4]Oak Ridge National Laboratory, Oak Ridge Tennessee, USA

Work supported by
the U.S. Department of Energy
under DE-AC01-09CH11466, DE-FG02-07ER54917, DE-FC02-04ER54698,
and DE-AC05-00OR22725

GENERAL ATOMICS PROJECT 30200
OCTOBER 2014

GENERAL ATOMICS

Full-f Neoclassical Simulations Toward a Predictive Model for H-mode Pedestal Ion Energy, Particle and Momentum Transport

EX/P2-24

D.J. Battaglia 1), J.A. Boedo 2), K.H. Burrell 3), C.S. Chang 1), J.M. Canik 4), J.S. deGrassie 3), S.P. Gerhardt 1), B.A. Grierson 1), R.J. Groebner 3), R. Maingi 1), and S.P. Smith 3)

e-mail: dbattagl@pppl.gov

1) Princeton Plasma Physics Laboratory, P.O. Box 451, Princeton, NJ 08543, USA
2) University of California San Diego, 9500 Gilman Dr., La Jolla, CA 92093-0417, USA
3) General Atomics, P.O. Box 85608, San Diego, CA, 92186-5608, USA
4) Oak Ridge National Laboratory, Oak Ridge, TN 37831, USA

Abstract. Energy and particle transport rates are decoupled in the H-mode edge since the ion thermal transport rate is primarily set by the neoclassical transport of the deuterium ions in the tail of the thermal energy distribution, while the net particle transport rate is set by anomalous transport of the colder bulk ions. Ion orbit loss drives the energy distributions away from Maxwellian, and describes the anisotropy, poloidal asymmetry and local minimum near the separatrix observed in the T_i profile. Non-Maxwellian distributions also drive large intrinsic edge flows, and the interaction of turbulence at the top of the pedestal with the intrinsic edge flow can generate an intrinsic core torque. The primary driver of the radial electric field (E_r) in the pedestal and scrape-off layer (SOL) are kinetic neoclassical effects, such as ion orbit loss of tail ions and parallel electron loss to the divertor. This paper describes the first multi-species kinetic neoclassical transport calculations for ELM-free H-mode pedestal and scrape-off layer on DIII-D using XGC0, a 5D full-f particle-in-cell drift-kinetic solver with self-consistent neutral recycling and sheath potentials. Quantitative agreement between the flux-driven simulation and the experimental electron density, impurity density and orthogonal measurements of impurity temperature and flow profiles is achieved by adding random-walk particle diffusion to the guiding-center drift motion. This interpretative technique quantifies the role of neoclassical, anomalous and neutral transport to the overall pedestal structure, and consequently illustrates the importance of including kinetic effects self-consistently in transport calculations around transport barriers.

1. Introduction

The high-confinement mode [1], or H-mode, is an attractive operating regime for future fusion reactors where an edge transport barrier leads to a pressure pedestal, consequently reducing the size and cost of the reactor. The multi-scale self-organization of the H-mode pedestal is qualitatively understood; however the first-principles models necessary for its quantitative prediction and optimization are an active area of research [2]. This paper describes recent progress in leveraging petascale computational resources and high-fidelity diagnostic measurements to self-consistently quantify the role of neoclassical, anomalous and neutral transport processes in the self-organization of the H-mode pedestal [3]. The ability of the simulation to simultaneously capture the observed density, temperature, electric field and parallel flow in the H-mode edge represents a major step toward the development of a quantitative predictive tool for optimizing the boundary plasma in nuclear fusion devices.

The reduction in turbulent transport observed in the H-mode pedestal [4] suggests that ion neoclassical transport becomes important, similar to what is observed with internal transport barriers in the plasma core [5]. However, this hypothesis is difficult to test using analytical neoclassical theory since kinetic, non-local and ion-neutral effects become significant in the H-mode pedestal. These effects lead to non-Maxwellian ion distributions and pitch-energy dependent transport rates within the pedestal, motivating the development of full-f transport simulations for predicting and optimizing the self-organization of the tokamak edge.

Radial drift excursions of the ions are considerably larger than electrons and are typically on the order of the pedestal width. A subset of ions in the tail of the thermal ion energy distribution has sufficiently large orbit excursions that the collisionless orbits intersect a wall (i.e., ion orbit loss) [6]. This loss mechanism is non-ambipolar, meaning the ion and electron orbit loss rates are not automatically balanced. Consequently, E_r is constrained to the value that reduces ion orbit loss enough to maintain ambipolar transport across the separatrix [7]. Similarly, the electron parallel loss rate along open field lines to the wall in the scrape-off layer (SOL) is much larger than the ion loss rate and a sheath develops to maintain ambipolar particle loss to the wall. The preferential loss of high-energy ions from the confined plasma has a significant impact on energy and momentum transport, with little impact on particle transport, leading to a decoupling of the energy, particle and momentum transport rates. Consequently, the evolution and saturation of the temperature, density and rotation profiles can differ in the H-mode pedestal. Another implication is that the non-Maxwellian ion distributions lead to profile characteristics that are not supported by fluid transport models, especially at low-collisionallity. For example, the ion temperature (T_i) profile will be anisotropic ($T_{i,para} \neq T_{i,perp}$) and have a local minimum near the separatrix, and the parallel flow will have an intrinsic offset flow that is large and in the co-I_p direction at the outboard midplane. This paper presents examples of the quantitative agreement between the predictions of kinetic neoclassical theory and experimental measurements made on DIII-D. The results motivate the continued development of full-f transport calculations toward a fully predictive first-principles model of the H-mode pedestal.

2. QH-mode pedestal transport calculations using XGC0

An attractive operating regime for future burning plasma tokamak operations is the quiescent H-mode (QH-mode) regime where sufficient edge toroidal flow shear is maintained to stabilize kink-peeling instabilities at finite amplitude [8,9]. The mode provides additional particle transport such that the pedestal is maintained at the kink-peeling stability limit while

avoiding any detectable ELMs and preventing the accumulation of impurities. The steady-state conditions are well suited for studying pedestal transport since diagnostics can employ large time integrations and the spatial resolution of measurements with fixed diagnostic views can be improved using gradual motions in the radial position of the plasma boundary (i.e., an edge sweep). The XGC0 numerical simulations presented in this letter are compared to previously published results from Burrell et al. that employed an edge sweep to collect high-resolution measurements of the QH-mode pedestal on the DIII-D tokamak [10].

XGC0 is a 5D (3D physical space and 2D in velocity space: $v_{\|}, v_{\perp}$) drift-kinetic multi-species (e^-, D^+, C^{6+}, D^0, C^0) particle-in-cell solver for a realistic magnetic geometry [11]. It is highly parallelized (typically using order 1000 processors) in order to efficiently follow the drift motion of order 10 million particles undergoing mass-energy-momentum conserving collisions with a dynamic background plasma and neutral fluid. The simulation inputs, assumptions and mechanics are described in detail in [3] and references within. A typical solution domain for plasma edge simulations has an inner boundary at $\psi_N = (\psi-\psi_0)/(\psi_X-\psi_0) = 0.8$ and an outer boundary at the wall. To simulate the action of a sheath, electrons are reflected at the outer boundary. Once an ion guiding-center crosses the outer boundary, it is removed from the simulation along with the highest-energy reflected electrons. The lowest energy electrons removed from the simulation set the plasma potential on the open field line. The background neutral fluid is updated using a Monte-Carlo neutral penetration calculation that launches test neutrals from the locations ions were lost in order to mimic wall recycling.

XGC0 produces a flux-driven solution where the plasma profiles evolve from an initial guess to a steady-state solution consistent with the fluxes prescribed at the simulation boundaries. The flux-surface averaged neoclassical radial ion and electron fluxes are evaluated after each ion time step and, if they are unbalanced, the potential on the closed flux surface is adjusted accordingly (see eq. 4 in [11]). Thus, XGC0 computes the E_r required to maintain ambipolar neoclassical transport in light of kinetic effects, such ion orbit loss and wall sheaths.

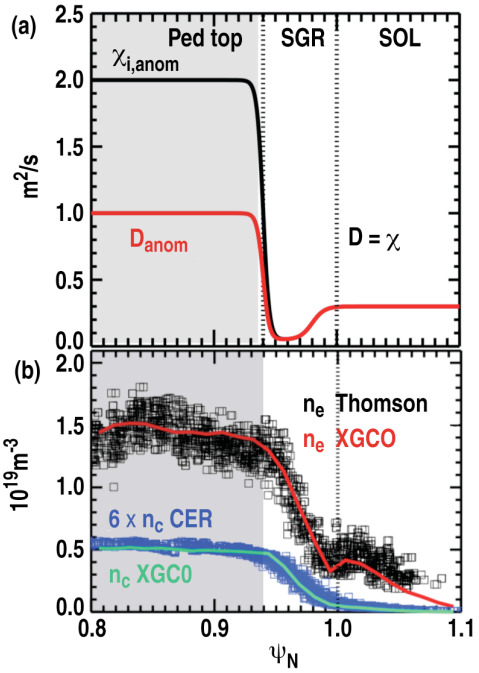

Fig. 1. (a) Effective XGC0 D_{anom} (red) and $\chi_{i,anom}$ at the outboard midplane from random-walk guiding center motion. (b) Synthetic diagnostic output for n_e (red) compared to experimental data (black) and the simulated C^{6+} density (green) compared to data (blue).

Past studies with XGC0 [11,12] have demonstrated that anomalous transport must be added to the kinetic neoclassical transport to adequately describe the experimentally observed profiles. The anomalous transport model used in this work is an energy-dependent random-walk perturbation to the spatial position of each guiding center. The effective D and χ due to the random-walk motion are input to the simulation as a 1D function versus ψ_N where the units are m^2/s at the outboard midplane. Figure 1(a) shows the 1D random-walk step-size profiles that are used for the QH-mode calculations. These profiles represent the transport that was added to the drift-kinetic transport solution in order to best match synthetic diagnostics in the simulation with the experimental measurements. There are three regions with different anomalous transport properties, in agreement with previous studies with interpretive and predictive H-mode transport models [2]. The electron thermal

transport is under-constrained in the XGC0 calculations since it is dependent on the user-defined anomalous χ_e and radiation cooling model. The relationship between the three regions of anomalous transport and the pedestal shape is illustrated by the electron density (n_e) and fully-stripped carbon density (n_C) profile in Fig. 1(b).

The difference between the shape of the n_e and n_C profiles is understood when considering the flux-surface averaged anomalous and neoclassical particle transport rates shown in Fig. 2. Neoclassical electron cross-field flux is small (red line, [Fig. 2(a)]), and thus the total electron particle flux (black line, [Fig. 2(a)]) in the pedestal is typically equal to the anomalous transport rate (blue line). However, the ion species have neoclassical particle fluxes that are significant, but offset, in the steep gradient region ([Fig. 2(b)]). In this case, the neoclassical deuterium flux is outward, while the neoclassical carbon flux is inward. These offsetting fluxes result in ion density pedestals that are species dependent. In the QH-mode discharges with a deep E_r well, the simulated in-out asymmetry of the carbon density within the pedestal is large and peaked on the high-field side (similar to the observed impurity density asymmetry in [13]). Furthermore, the neoclassical pinch of the carbon ions provides a mechanism for establishing the n_C pedestal with only neutral recycling as a source.

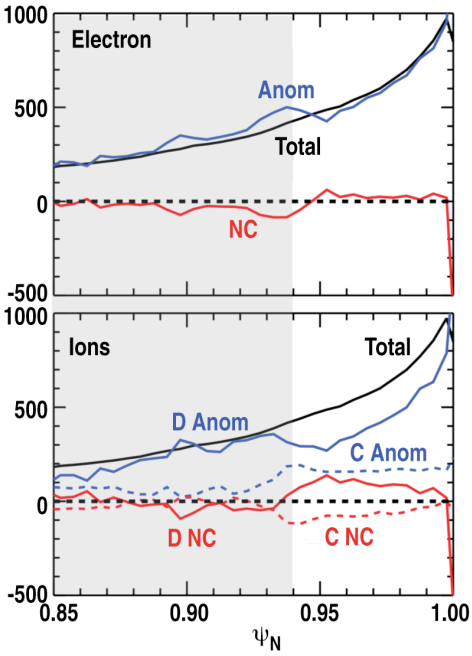

Fig. 2. (a) Total electron radial current in Amperes (black) equals the sum of anomalous (blue) and neoclassical (red) transport. (b) Total ion radial current (black) equals total electron current. Anomalous (blue) and neoclassical (red) contributions are shown for C^{6+} (dotted) and deuterium (solid).

The random-walk model is designed to be ambipolar and thus the anomalous electron radial current is by definition equal to the sum of the anomalous ion radial currents (blue solid lines in Fig. 2). XGC0 dynamically evolves the electrostatic potential (Φ) on each flux surface in order to balance the electron and ion neoclassical currents (red solid lines) inside the separatrix. The simulated E_r at the outboard midplane resulting from the self-consistent Φ that maintains ambipolar neoclassical transport is shown in Fig. 3 (red line). The E_r inferred from single-fluid force balance ($E_r = (Z_i e n_i)^{-1}\nabla P_i - v_{\theta i}B_\phi + v_{\phi i}B_\theta$) using the C^{6+} CER profiles is also shown in Fig. 3 (shaded region reflects measurement error). The E_r profile inferred using the single-fluid force balance equation assumes the energy distribution is Maxwellian and the profile smoothing from finite Larmor radius (FLR) effects and diagnostic response is small. The discrepancy between the E_r computed by XGC0 and the inferred E_r from force-balance is described by the breakdown of these assumptions in the pedestal region.

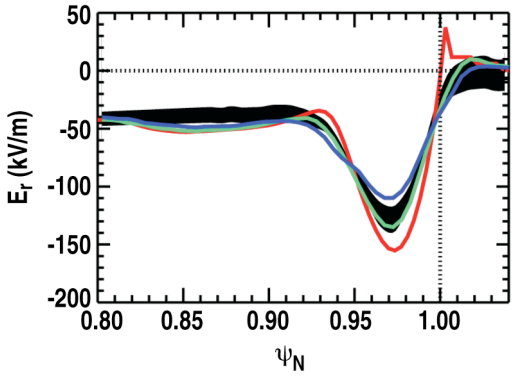

Fig. 3 E_r inferred from force balance with CER C^{6+} profiles (black) compared to the simulated E_r using XGC0 (red) and the resulting fluid force balance approximations for E_r using C^{6+} (green) and D^+ (blue) profiles.

XGC0 uses a simple gyro-motion model to approximate the gyro-averaged Φ that contributes to the gyro-center motion. The difference between the gyro-averaged Φ and the value at the

gyro-center becomes significant for high-energy deuterium ions, where the variations in Φ in the pedestal are on the order of the Larmor radius, especially around the separatrix. Furthermore, the energy distribution of deuterium ions is farther from Maxwellian than impurity ions due to their larger banana orbits. As a result, the single-fluid force balance approximation for deuterium using the simulated XGC0 profiles (blue line in Fig. 3) significantly underestimates the depth of the E_r well. The single-fluid force balance approximation for E_r using the simulated C^{6+} profiles with the finite diagnostic response of CER (green line) is closer to the true E_r in the plasma (red line) and in good agreement with the experimental profile (black shaded region).

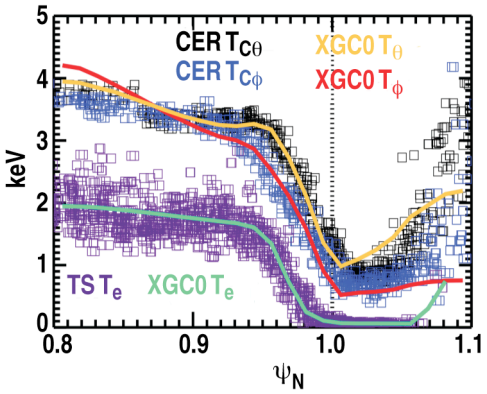

Fig. 4 XGC0 synthetic diagnostic temperatures (solid lines) compared to measurements (squares).

The C^{6+} temperature is measured at the outboard midplane using both vertically and tangentially viewing charge-exchange recombination (CER) systems on DIII-D. The temperature profiles measured by the orthogonal views are different (anisotropic) in the steep-gradient region of high-T_i, low-collisionallity QH-mode pedestals and the XGC0 simulation quantitatively reproduces this observation (Fig. 4). The simulation is also in qualitative agreement with the observed increase in the C^{6+} temperature in the SOL at the outboard midplane due to a population of high-energy trapped particles that originate from the top of the pedestal and "hang out" into the far SOL [14]. Agreement between the simulated and measured T_e at the Thomson scattering location is also shown in Fig. 4; however, this agreement is unremarkable since the model is under constrained for electron thermal transport.

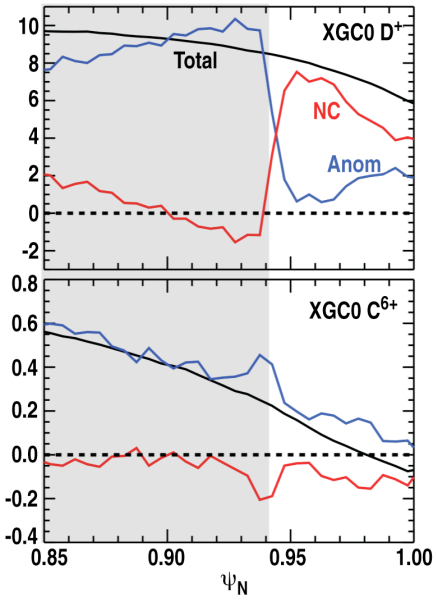

Fig. 5 (a) Total radial ion heat flow in MW carried outward by deuterium (black) and the respective contributions from anomalous (blue) and neoclassical (red) transport. (b) Same information for C^{6+} ions.

The QH-mode discharge was heated with 9.1 MW of counter-I_p neutral beam injection and about 1 MW of ohmic heating. The corresponding core heat fluxes used for the XGC0 simulations (based on core transport modeling) are 6.5 MW of deuterium heating, 0.5MW of carbon heating and 1 MW of electron heating. Figure 5 shows the flux-surface averaged ion energy flux for deuterium and carbon. The ion heat flow is predominately anomalous at the top of the pedestal ($\psi_N < 0.94$), and predominately neoclassical in the steep-gradient region, especially for deuterium. About 9 MW of heat flows through the pedestal via the ions, with about 3 MW lost to collisions with electrons and neutrals and the remaining 6 MW transported to the SOL by deuterium ions.

This kinetic neoclassical calculation indicates that a small population of high-energy deuterium ions in the tail of the thermal energy distribution transports most of the energy across the H-mode pedestal on drift orbits, while the particle transport is primarily dictated by anomalous transport. Separation of particle and energy transport processes across the pedestal

is often seen in ELM-free tokamak regimes, including QH-mode, where an edge perturbation from a mode increases the particle flux through the pedestal with minimal impact on the energy transport. This is consistent with the result that particle transport, and thus the density pedestal, are more affected by anomalous transport than energy transport and the corresponding temperature profile. The separation of energy and particle transport processes can also play a role in the evolution of the H-mode pedestal following the L-H transition or an ELM where the temperature and density pedestals will often evolve on different timescales.

Figure 6a shows the computed deuterium energy distribution (black lines) at the top of the H-mode pedestal ($0.88 < \psi_N < 0.9$) at the outboard midplane. The orange section is the loss hole where an ion with a given energy and pitch is on a collisionless ion orbit that directly impacts the wall (primarily in the divertor). The dashed blue lines are contours of constant energy in the counter-I_p rotation frame of the cold bulk ions (i.e., shifted Maxwellian). This rotation is maintained by 3 Nm of torque applied by the neutral beam injection (NBI). The green dashed lines are the approximate trapped-passing boundary in the presence of finite E_r (eq. A.6 in [15]). Kinetic effects lead to a parallel velocity distribution (Fig. 6b black line) where a Gaussian fit of the parallel flow (red) is more co-I_p than the cold bulk ion flow (blue). This intrinsic co-I_p edge flow at the outboard midplane has been observed in many tokamaks across a variety of operational regimes. Figure 7 illustrates the quantitative agreement between the flows predicted by XGC0 at the outboard midplane and the measured carbon flows. The simulation captures the transition from counter-I_p toroidal flows in the core to co-I_p flow past the separatrix and the finite poloidal flow for C^{6+} (red lines compared to black points). Deuterium flows are expected to be significantly different than C^{6+} and quantitative comparisons are underway to test these predictions against the measurements from the novel deuterium CER system under development at DIII-D [16].

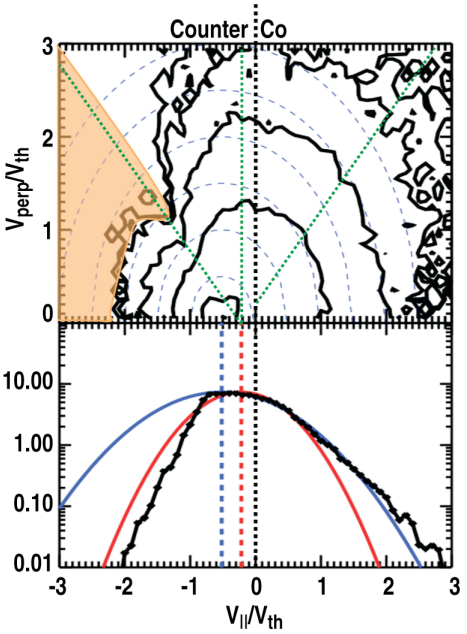

Fig. 6 (a) D^+ density in velocity space at the top of pedestal at the outboard midplane (black lines). Dashed blue lines are contours of constant energy centered on bulk parallel flow. Green lines are trapped-passing boundaries and orange region is the loss hole. (b) Total D^+ density (A.U.) versus normalized parallel flow velocity (black). Blue line is Gaussian fit to co-I_p ions and red line is Gaussian fit of all ions.

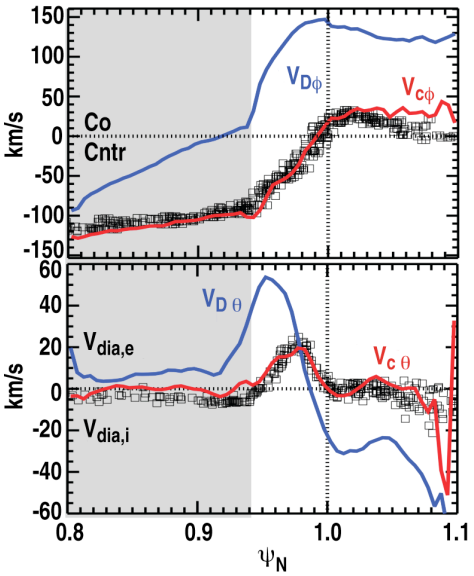

Fig. 7 XGC0 simulated flows for C^{6+} (red) and D^+ (blue) at outboard midplane compared to C^{6+} measurements (black).

3. Intrinsic torque in ECH heated H-mode

Tokamak plasmas often develop finite toroidal rotation when no external torque is applied. There is a growing need to understand the nature of the self-generated torque responsible for this rotation (i.e., intrinsic torque) since it is expected to be on the same order as the external

torque sources in future devices, such as ITER. The intrinsic rotation of C^{6+} ions measured with CER and D+ ions measured with a reciprocating Mach probe at the outboard midplane of DIII-D for a H-mode discharge heated with electron cyclotron heating (ECH) is shown in Fig. 8. Both ion species are rotating toroidally in the direction of the plasma current (co-I_p), however the magnitudes are significantly different near the separatrix.

XGC0 simulations with only heat and particle flux from the core boundary (no momemtum flux) develop an intrinsic flow consistent with the observed flows. Figure 8 illustrates that flows predicted by XGC0 at the outboard midplane (red lines) are in good agreement with the measurements for $\psi_N > 0.9$, but under predict the flow for $\psi_N < 0.9$. The flux-surface averaged flows (blue lines in Fig. 8) are non-zero, indicating that the plasma has generated a net co-I_p flow.

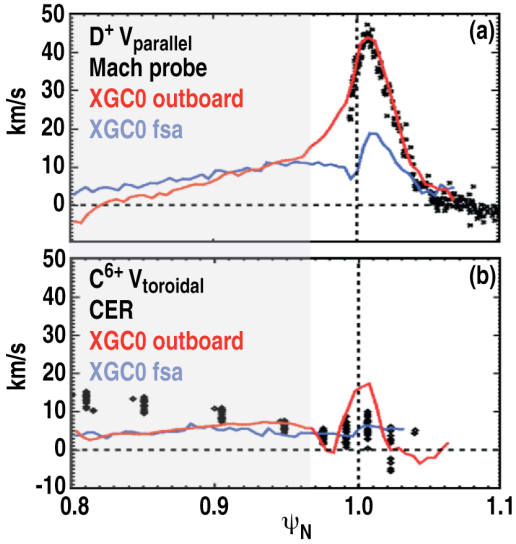

Fig. 8. Predicted intrinsic flows at outboard midplane for an ECH-heated discharge using XGC0 (red lines) compared to measured (a) D^+ parallel flow and (b) C^{6+} toroidal flow (black points). Blue lines are flux-surface averaged flows. Ion momentum transport is predominately anomalous in gray region, neoclassical in white region.

Agreement with density profiles requires the random-walk guiding center diffusion to have $D_{anom} \sim 0.2$ m^2/s for $\psi_N < 0.965$ and $D_{anom} \sim 0.01$ m^2/s outside of this flux surface. Thus, the anomalous transport around the separatrix is small and the magnitude of the co-I_p flow in this region is primarily due to neoclassical and ion-neutral physics. The poloidal asymmetry (essentially the difference between the red and blue curves) is largest around the separatrix where the large E_r and pressure gradients lead to a neoclassical Pfrish-Schluter flow.

Core intrinsic torque is generated when the core anomalous transport interacts with the edge neoclassical flows at the top of the pedestal ($\psi_N \sim 0.965$). This interface has a large gradient in D_{anom}, which has been shown to lead to intrinsic co-I_p torque due to the random-walk motion of passing particles into a loss hole [17]. The propagation of the co-I_p flow inside of the top of the pedestal depends on the details of the anomalous transport and the disagreement between XGC0 and the measurements in this region suggests the random-walk model in XGC0 does not capture the physics leading to the momentum pinch.

4. Future Work and Summary

ELMy H-mode discharges on DIII-D and other standard aspect-ratio tokamaks have demonstrated that the pedestal pressure stability limits are in good agreement with the limits derived from peeling-ballooning stability theory and the kinetic ballooning mode (KBM) onset criteria [18]. Pedestal transport modeling, such as what has been demonstrated with XGC0, is required to predict and optimize the density and temperature contributions to the maximum stable pressure. Ongoing work with XGC0 is aimed at identifying the separate scaling of energy and particle transport mechanisms with I_p to provide insight into the expected scaling of the density and temperature pedestal heights at the maximum stable pressure in future high-current devices.

Present efforts are also focused on extending the XGC0 simulations to the low-aspect ratio geometry of NSTX in order to study the double ion transport barrier observed on NSTX in Extended Performance H-mode (EPH-mode) [19]. Ion energy transport is neoclassical everywhere in the confined plasma in H-mode due to the large banana orbit widths in spherical tokamaks. In EPH-mode, the ion thermal confinement quickly improves in a region of enhanced toroidal velocity shear. Initial studies with XGC0 confirm that a transient increase in the toroidal rotational shear can initiate a positive feedback loop that leads to the enhanced confinement of counter-current main-ion tail ions and improved ion energy confinement.

XGC0 leverages recent advances in high-performance computing to quantify the contribution of neoclassical transport, including the significant finite-orbit-width effects, on H-mode pedestal transport. Quantitative agreement with the measured T_i, flow, E_r and Z_{eff} profiles for a wide range of H-mode conditions on DIII-D and NSTX and the observed separation of pedestal particle and energy transport provide confidence that full-f neoclassical transport calculations with self-consistent neutral recycling and a simple random-walk anomalous transport model captures the important physics of the H-mode pedestal transport. The development of a quantitative flux-driven transport solution for the H-mode pedestal represents a crucial step toward a predictive model and provides a tool for inferring the global pedestal parameters based on limited edge diagnostic coverage.

5. Acknowledgement

This material is based upon work supported by the U.S. Department of Energy, Office of Science, Office of Fusion Energy Sciences, using the DIII-D National Fusion Facility, a DOE Office of Science user facility, under Awards DE-AC02-09CH11466, DE-FG02-07ER54917, DE-FC02-04ER54698, and DE-AC05-00OR22725. DIII-D data shown in this paper can be obtained in digital format by following the links at https://fusion.gat.com/global/D3D_DMP.

References

[1] F. Wagner (2007) *Plasma Phys. Control. Fusion* **49,** B1–B33
[2] J.D. Callen *et al* (2010) *Nucl. Fusion* **50,** 064004
[3] D.J. Battaglia *et al* (2014) *Phys. Plasmas* **21,** 072508
[4] P. Terry (2000) *Rev. Modern Phys.* **72**
[5] J. Connor *et al* (2004) *Nucl. Fusion* **44**, R1–R49
[6] A. Chankin *et al* (1993) *Nucl. Fusion* **33,** 1459
[7] C.S. Chang (2002) *Phys. Plasmas* **9,** 3884
[8] K. Burrell *et al* (2005) *Phys. Plasmas* **12,** 056121
[9] P. Snyder *et al* (2007) *Nucl. Fusion* **47,** 961
[10] K. Burrell *et al* (2004) *Plasma Phys. Control. Fusion* **46**, A165–A178
[11] C.S Chang *et al* (2004) *Phys. of Plasmas* **11,** 2649
[12] A.Y. Pankin *et al* (2013) *Phys. Plasmas* **20,** 102501
[13] R.M. Churchill *et al* (2013) *Nucl. Fusion* **53,** 122002
[14] C. Lasnier and K. Burrell (2003) *J. Nucl. Material.* **313,** 904–8
[15] J.S. Degrassie *et al* (2009) *Nucl. Fusion* **49,** 085020
[16] B.A. Grierson *et al* (2012) Phys. Plasmas **19,** 056107
[17] Stoltzfus-Dueck (2012) *Phys. Plasmas* **19,** 055908
[18] P.B. Snyder *et al* (2009) *Phys. Plasmas* **16,** 056118
[19] S.P. Gerhardt *et al* (2014) *Nucl. Fusion* **54,** 083021